



# Effect of stacking fault energy on irradiation damage in reduced activation high entropy alloys

N. Hashimoto<sup>a,\*</sup>, E. Wada<sup>b</sup>, H. Oka<sup>a</sup>

<sup>a</sup> Faculty of Engineering, Hokkaido University, Sapporo, 060-8628, Japan

<sup>b</sup> Graduate School of Engineering, Hokkaido University, Sapporo, 060-8628, Japan

## ARTICLE INFO

### Article history:

Received 30 November 2021

Revised 4 March 2022

Accepted 23 April 2022

Available online 5 May 2022

### Keywords:

High entropy alloy

Stacking fault energy

Irradiation

Microstructure evolution

## ABSTRACT

In order to investigate the effect of stacking fault energy on microstructural evolution in reduced activation high entropy alloys, electron and/or Au<sup>+</sup> ion irradiation was performed to the Co-free FCC-type FeCr<sub>0.8</sub>Ni<sub>x</sub>Mn<sub>y</sub> ( $x, y = 1, 1.3, 1.5$ ) alloys. TEM observation of the 5%-deformed FeCr<sub>0.8</sub>Ni<sub>x</sub>Mn<sub>y</sub> alloys revealed the increase in the stacking fault energy with increasing both Ni and Mn concentration. In addition, FeCr<sub>0.8</sub>Ni<sub>1.5</sub>Mn<sub>1.5</sub> had the highest stacking fault energy, which was much higher value than that of 316SS. Furthermore, the yield strength and the elongation of deformed FeCr<sub>0.8</sub>Ni<sub>x</sub>Mn<sub>y</sub> also showed the Ni and Mn concentration dependence. The electron irradiation at 400 °C resulted in the formation of black dots, self-interstitial atom faulted loops, but no observable voids in all the FeCr<sub>0.8</sub>Ni<sub>x</sub>Mn<sub>y</sub> alloys. The comparison of microstructural evolution revealed less faulted loop formation and growth in FeCr<sub>0.8</sub>Ni<sub>1.3</sub>Mn<sub>1.3</sub> and FeCr<sub>0.8</sub>Ni<sub>1.5</sub>Mn<sub>1.5</sub> alloys. From these results, it is suggested that FeCrNiMn-based high entropy alloys would be developed as high irradiation resistant materials by controlling the stacking fault energy with optimized element concentration.

© 2022 Elsevier B.V. All rights reserved.

## 1. Introduction

In the last decade, the high entropy alloys (HEAs) have been paid attention due to their high strength, ductility, wear resistance, high temperature softening resistance and corrosion resistance compared to conventional metallic material [1–4]. Some of HEAs have been reported as candidate materials for nuclear applications due to their high radiation resistance and corrosion resistance especially at elevated temperatures [5–7]. On the radiation resistance of HEAs, Lu et. al. firstly reported the enhanced swelling resistance at 500 °C in FCC-type CoCrFeNiMn alloy attributed to the tailored interstitial defect cluster motion from a long-range one-dimensional mode to a short-range three-dimensional mode, which leads to enhanced point defect recombination [8]. Yang also reported [9] that the irradiated HEAs exhibited a better irradiation tolerance than pure metal at 500 °C, including slower accumulation of irradiation-induced structural damage and lower void swelling, probably due to both the compositional complexity and alloying elements. Generally, FCC-type materials tend to have a low stacking fault energy (SFE) compared to BCC-type materials, leading to the formation of stacking fault-type defects, such as stacking

fault tetrahedron (SFT) and faulted Frank loops (faulted FLs) in matrix, when irradiated in a wide temperature range [10–16]. Those stacking fault-type defects, especially FLs, would be a key of degradation of FCC-type materials under irradiation. Chen et. al. investigated the microstructure change in CoCrFeNiMn alloy under irradiation at 300 °C, found that the size and density evolutions of dislocation loops in the HEA were similar to that in 316H stainless steel [17]. And it is suggested that the loop size and density might be related to the differences in vacancy mobility [17]. On the mobility of point defects in CoCrFeNiMn alloy, Hashimoto and Ono conducted the *in-situ* electron irradiation experiment and the positron annihilation analysis revealed that Co, Ni, Mn, and Al atoms could affect the vacancy mobility in HEAs but not the interstitial mobility [18]. For the effect of element content on SFE, Mn would play an important role for the change in the SFE [19]. However, it is noted that these studies on the irradiation resistance were conducted to Co-including FCC-type HEAs.

Concerning about the irradiation response on Co-free HEAs, neutron irradiation experiment revealed that CrFeMnNi HEA showed similar behavior to Fe-Cr-Ni in mechanical strength, phase stability and the annealing of vacancy-type defects, whereas the solute diffusion is slower up to 700 °C [20]. Parkin et. al. also investigated the irradiation damage in CrFeMnNi-type HEA and found the difference in loop growth kinetics attributed to the difference in Mn-content [21]. This work suggested the detail

\* Corresponding author.

E-mail address: [hashimoto@eng.hokudai.ac.jp](mailto:hashimoto@eng.hokudai.ac.jp) (N. Hashimoto).

**Table 1**  
Chemical composition of FeCr<sub>0.8</sub>Ni<sub>x</sub>Mn<sub>y</sub> alloys (at%).

	Fe	Cr	Ni	Mn	C	N	O
FeCr <sub>0.8</sub> NiMn	26.3	21.1	26.3	26.3	0.002	0.007	0.044
FeCr <sub>0.8</sub> NiMn <sub>1.3</sub>	24.4	19.5	24.4	31.7	0.002	0.005	0.054
FeCr <sub>0.8</sub> Ni <sub>1.3</sub> Mn <sub>1.3</sub>	22.7	18.3	29.5	29.5	0.003	0.006	0.035
FeCr <sub>0.8</sub> Ni <sub>1.5</sub> Mn <sub>1.5</sub>	20.8	16.6	31.3	31.3	0.002	0.005	0.045

analysis on the SFE as a useful parameter for determining the irradiation resistance of FCC-type HEAs as well as their strength, ductility, and strain-hardening behavior. In this study, therefore, we focused on Co-free FCC-type FeCrNiMn-based HEAs and investigated the effect of element content on the SFE. Furthermore, in order to clarify the effect of SFE on irradiation damage evolution microstructural changes of those HEAs were investigated by *in-situ* irradiation experiment.

## 2. Experimental procedure

The materials used in this study are FCC-type single phase alloys; FeCr<sub>0.8</sub>Ni<sub>x</sub>Mn<sub>y</sub> ( $x, y = 1, 1.3, 1.5$ ). The FeCr<sub>0.8</sub>Ni<sub>x</sub>Mn<sub>y</sub> were prepared by arc-melting method in high-purity argon atmosphere, followed by solution annealing at 1160 °C for 24 h. The chemical composition of all the alloys was listed in Table 1. The chemical composition of C, N, and O were analyzed by the combustion infrared absorption method, the inert gas melting-thermal conductivity method, and the inert gas melting-infrared absorption method. For the estimation of SFE, all the alloys were cold-rolled down to 0.25 mm in thick, then punched out for tensile test (SS-J2 type with a gage length of 5 mm). Tensile test was conducted at room temperature, and then, the deformed region was cut and electro-polished to provide for TEM observation. For the *in-situ* irradiation experiments and microstructure observation, 3 mm $\phi$  TEM disks were punched out from the as-annealed samples and electro-polished. Before the irradiation experiments, macro- and microstructures of the alloys were investigated by using SEM (FE-SEM JEOL JSM6500F) and XRD (Rigaku Fully automatic horizontal multipurpose X-ray diffractometer). *In-situ* electron irradiation experiment was performed at 400 °C to 0.2 dpa at the dose rate of  $1 \times 10^{-3}$  dpa/s using the Multi-beam High Voltage Electron Microscope (HVEM) operated at 1.25 MeV at Hokkaido University. The 8MeV Au<sup>+</sup> ion irradiation was also performed at 500 °C up to 72 dpa at the dose rate of  $6.8 \times 10^{-4}$  dpa/s for a part of samples by the Takasaki Ion Accelerator for Advanced Radiation Application (TIARA) of the National Institute for Quantum Science and Technology (QST).

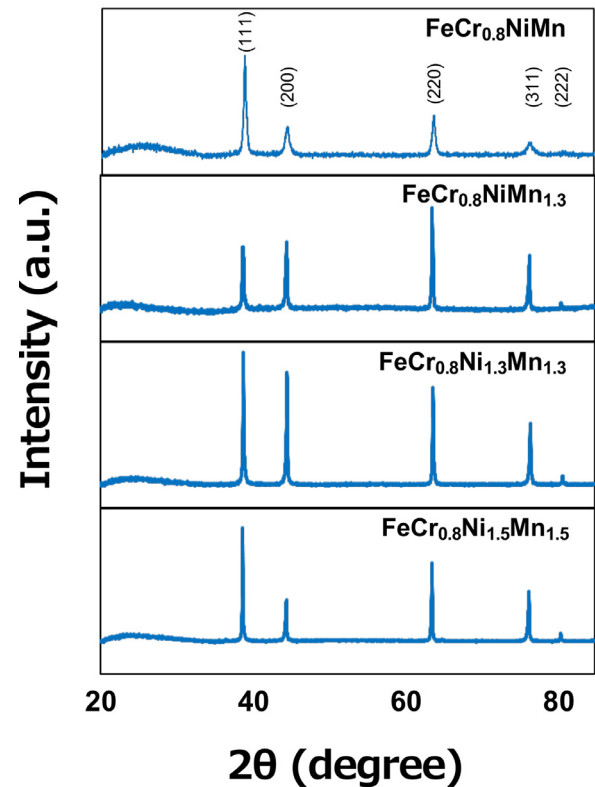


**Fig. 1.** XRD results of FeCr<sub>0.8</sub>Ni<sub>x</sub>Mn<sub>y</sub> alloys after solution annealing.

## 3. Results

### 3.1. Structure and stacking fault energy of FeCr<sub>0.8</sub>Ni<sub>x</sub>Mn<sub>y</sub>

Fig. 1 shows the XRD results of FeCr<sub>0.8</sub>Ni<sub>x</sub>Mn<sub>y</sub> alloys after solution annealing. The profile showed the peaks from (111), (200), (220), (311) and (222) of FCC structure only, indicating that each alloy has the FCC-type single phase structure. In addition, EDS mappings of the alloys showed no concentration gradient or segregation in matrix. Fig. 2 shows the electron backscatter diffraction (EBSD) maps of the FeCr<sub>0.8</sub>Ni<sub>x</sub>Mn<sub>y</sub> alloys. The average grain sizes of FeCr<sub>0.8</sub>NiMn, FeCr<sub>0.8</sub>NiMn<sub>1.3</sub>, FeCr<sub>0.8</sub>Ni<sub>1.3</sub>Mn<sub>1.3</sub>, and FeCr<sub>0.8</sub>Ni<sub>1.5</sub>Mn<sub>1.5</sub> were 92, 78, 72, and 77  $\mu$ m, respectively, which would be comparable for the comparison of their mechanical properties. The solution-annealed FeCr<sub>0.8</sub>Ni<sub>x</sub>Mn<sub>y</sub> alloys included no precipitates but dislocation lines or segments ( $< 10^{13}$  m<sup>-2</sup>) in matrix. The 5%-deformed FeCr<sub>0.8</sub>Ni<sub>x</sub>Mn alloys included more disloca-

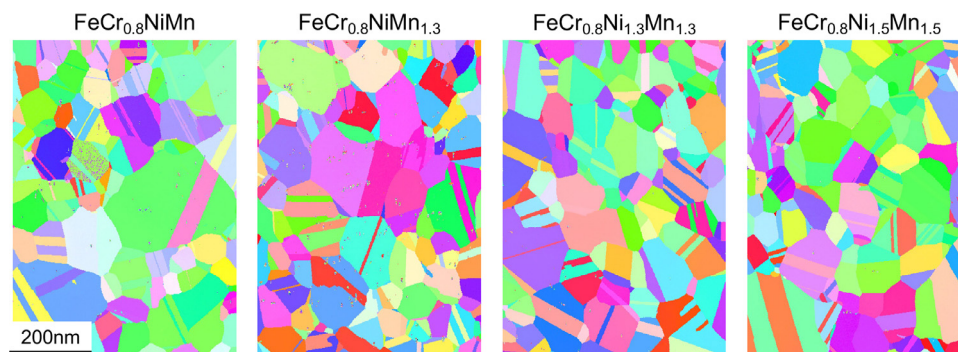


**Fig. 2.** Electron backscatter diffraction (EBSD) maps of FeCr<sub>0.8</sub>Ni<sub>x</sub>Mn<sub>y</sub> alloys.

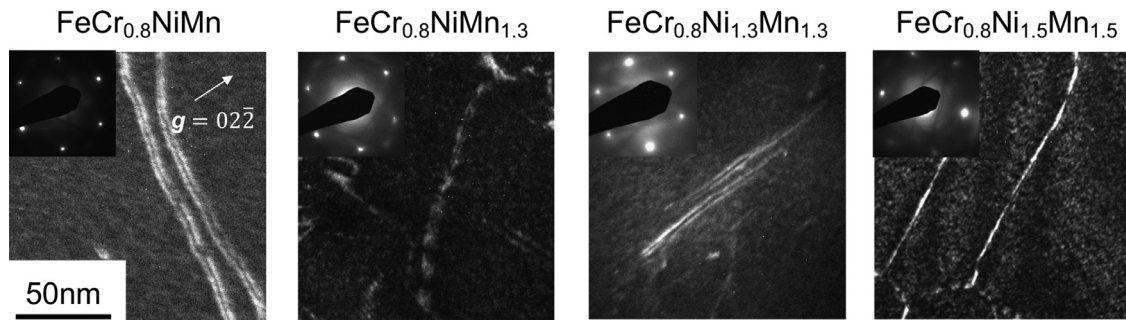


Fig. 3. WBDF images of dissociated dislocations in the deformed  $\text{FeCr}_{0.8}\text{Ni}_x\text{Mn}_y$  alloys.

Table 2

Shear modulus and Poisson's ratio of the alloys, measured by resonant ultrasound spectroscopy.

	Shear modulus / GPa	Poisson's ratio
$\text{FeCr}_{0.8}\text{NiMn}$	62.7	0.30
$\text{FeCr}_{0.8}\text{NiMn}_{1.3}$	59.5	0.30
$\text{FeCr}_{0.8}\text{Ni}_{1.3}\text{Mn}_{1.3}$	49.9	0.30
$\text{FeCr}_{0.8}\text{Ni}_{1.5}\text{Mn}_{1.5}$	51.1	0.32

tion lines ( $< 10^{14} \text{ m}^{-2}$ ) and were used for the estimation of the stacking fault energy. Fig. 3 shows the WBDF images of dissociated dislocations in the deformed  $\text{FeCr}_{0.8}\text{Ni}_x\text{Mn}_y$  alloys. Those images were taken in the beam condition of  $B = 111$ ,  $g = 022$ , and  $(g/5g)$ . The dissociation width of partial dislocations is defined as a function of the angle between the dislocation line and the total Burgers vector. The separation distance ( $d$ ) and the angle ( $\beta$ ) between the dislocation and the Burgers vector of full dislocation of these three alloys are measured. The stacking fault energy:  $\gamma$  can be expressed the following equation,

$$\gamma = \frac{Gb_p^2}{8\pi d} \left( \frac{2-\nu}{1-\nu} \right) \left( 1 - \frac{2\nu \cos(2\beta)}{2-\nu} \right)$$

where,  $G$  is the shear modulus,  $b_p$  is the magnitude of the  $1/6\langle a \rangle 112$  partial dislocation Burgers vector ( $a$  is the lattice parameter determined by X-ray diffraction) and  $\nu$  is the Poisson's ratio. The Shear modulus and Poisson's ratio of the alloys, measured by resonant ultrasound spectroscopy, were listed in Table 2. Fig. 4 shows the estimated SFE values of  $\text{FeCr}_{0.8}\text{Ni}_x\text{Mn}_y$  alloys with some previous data points of CoCrFeNiMn type HEAs reported by Liu et al. [22] and Hashimoto et al. [19]. The SFE values of  $\text{FeCr}_{0.8}\text{Ni}_x\text{Mn}_y$  alloys are higher compared with CoCrFeNiMn type HEAs. Furthermore, the SFE value seemed to be increased with increasing Mn and Ni concentration. From Fig. 4, it seems that Ni concentration dependence on the SFE could be slightly larger than that of Mn.

### 3.2. Tensile property of $\text{FeCr}_{0.8}\text{Ni}_x\text{Mn}_y$

$\text{FeCr}_{0.8}\text{Ni}_x\text{Mn}_y$  alloys were tensile-tested at RT at the strain rate of  $10^{-4}$ . Fig. 5 shows the engineering stress - engineering strain curve of all the  $\text{FeCr}_{0.8}\text{Ni}_x\text{Mn}_y$  alloys. It is noted that the 0.2% proof stress ( $\sigma_{0.2}$ ) and the ultimate tensile strength (UTS) seem to be slightly increasing with increasing Mn and Ni contents, but the total elongation ( $\epsilon_t$ ) was almost the same among the alloys. And those values were comparable to that of 316H stainless steel [23].

### 3.3. Microstructural evolution in irradiated $\text{FeCr}_{0.8}\text{Ni}_x\text{Mn}_y$

$\text{FeCr}_{0.8}\text{Ni}_x\text{Mn}_y$  alloys were electron irradiated at  $1 \times 10^{-3}$  dpa/s to 0.2 dpa at 400 °C. In this irradiation condition, both self-

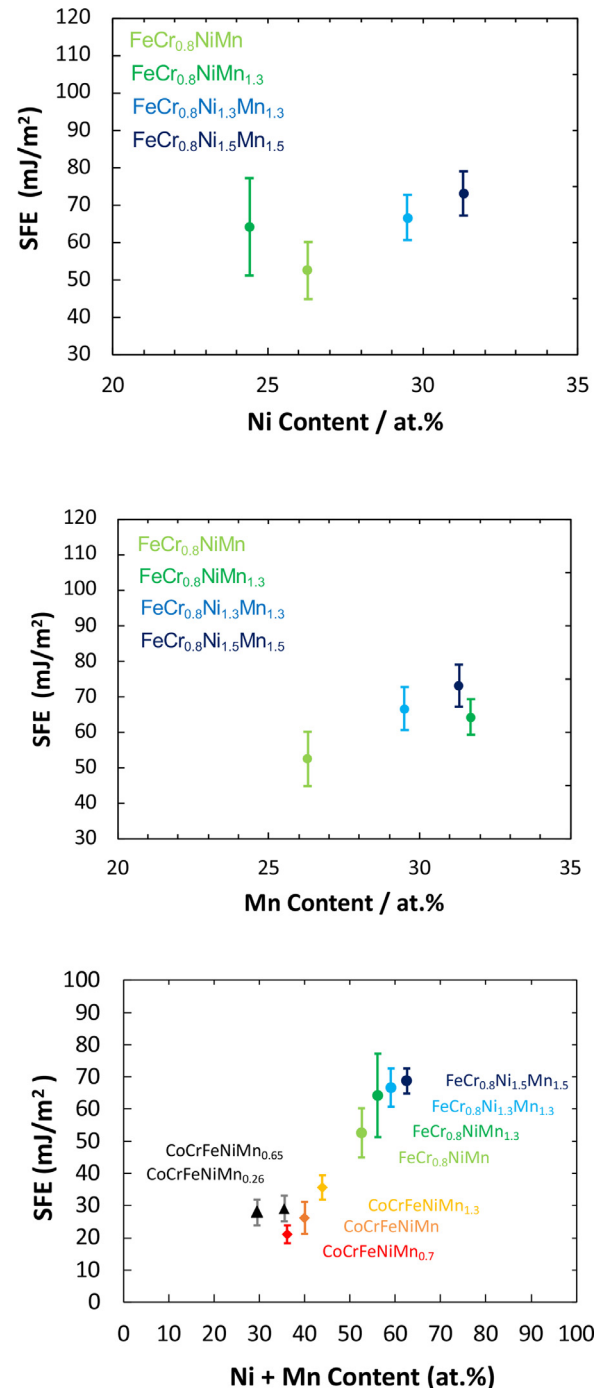


Fig. 4. Estimated SFE values of  $\text{FeCr}_{0.8}\text{Ni}_x\text{Mn}_y$  as a function of Ni and Mn content. The SFE values of CoCrFeNiMn<sub>x</sub> also plotted as comparison [19,22].



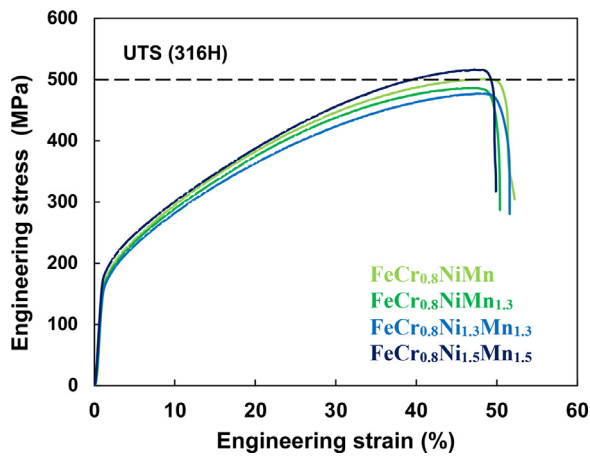


Fig. 5. The engineering stress - engineering strain curve of  $\text{FeCr}_{0.8}\text{Ni}_x\text{Mn}_y$  alloys tested at RT at the strain rate of  $10^{-4}$ .

interstitial atom (SIA) and vacancy can move appreciably [10]. All the alloys remained fully crystalline and retained their original FCC phase with no detectable second phase observed during irradiation experiment. Generally, the electron irradiation introduced point defects in materials, and then, microstructural evolution such as the formation and the growth of SIA cluster (black dot: BD), SIA faulted loops (FL), and cavities would be observed with increasing irradiation dose. Fig. 6 shows the damage microstructure of irradiated  $\text{FeCr}_{0.8}\text{Ni}_x\text{Mn}_y$  alloys. BDs and FLs were observed in the weak-beam dark-field (WBDF) images. The dark-field (DF) images from relrod showed only FLs on (111) plane. The irradiated  $\text{FeCr}_{0.8}\text{Ni}_{1.5}\text{Mn}_{1.5}$  indicated a low number density of ( $8.7 \times 10^{22} \text{ m}^{-3}$ ) and the average size (50 nm) of FL compared with the others and even 316SS [24]. A part of FLs could be unfaulted to SIA perfect loops (PL), however, the unfaulting process was not observed in this *in-situ* irradiation experiment. The critical size for unfaulting of the SIA FLs was not clear [25,26]. Assuming that the critical

unfaulting size is depending on the SFE, the SIA FL formation in irradiated  $\text{FeCr}_{0.8}\text{Ni}_x\text{Mn}_y$  alloys could be controlled by the Ni and Mn concentration. In addition, it is noted that no observable cavities were found in all the  $\text{FeCr}_{0.8}\text{Ni}_x\text{Mn}_y$  alloys. In order to investigate the formation of cavities and/or vacancy type clusters such as stacking fault tetrahedra (SFT), the  $\text{Au}^+$  ion irradiation at 500 °C up to 72 dpa was performed to  $\text{FeCr}_{0.8}\text{Ni}_{1.3}\text{Mn}_{1.3}$  alloy, however, both cavities and SFTs were not found in matrix and even at grain boundaries. Fig. 7 summarized the number density and the average size of FL in irradiated  $\text{FeCr}_{0.8}\text{Ni}_x\text{Mn}_y$ . It seems that the number density of FL was decreased with increasing Ni and Mn contents. While, the average size of FL would be almost the same among the  $\text{FeCr}_{0.8}\text{Ni}_x\text{Mn}_y$  alloys.

#### 4. Discussion

For the estimation of the SFE, Olson and Cohen model [27] can be applied. The formula is expressed as below.

$$\text{SFE} = 2\rho_A(\Delta G^{\text{FCC} \rightarrow \text{HCP}} + E^{\text{strain}}) + 2\sigma$$

where  $\rho_A$  is the atomic density of {111},  $\Delta G^{\text{FCC} \rightarrow \text{HCP}}$  is the difference of free energy before and after FCC  $\rightarrow$  HCP transformation,  $E^{\text{strain}}$  is the elastic strain energy of transformation, and  $\mu$  is the surface energy of FCC/HCP interface. The free energy calculation was performed with using PANDAT-2028 (CALPHAD). Fig. 8 shows that the free energy change of FCC and HCP in  $\text{FeCr}_{0.8}\text{Ni}_x\text{Mn}$  and  $\text{FeCr}_{0.8}\text{NiMn}_x$  as a function of Ni and Mn contents, respectively. It seems that the increase in Mn and Ni would increase the SFE in this experiment. As shown in Fig. 8,  $\Delta G^{\text{FCC} \rightarrow \text{HCP}}$  is increased with increasing Ni and Mn contents. Therefore, the thermodynamics calculation can support the experimental result of the change in SFE of  $\text{FeCr}_{0.8}\text{Ni}_x\text{Mn}_y$  alloys. In addition, Ni concentration dependence on the SFE seems to be slightly greater than that of Mn. Lu et al. investigated the effect of Ni and Mn on FeCrNi-based alloys with various Ni contents via quantum-mechanical first-principles calculations [28]. It is found that Mn increases the SFE at room temperature in high-Ni alloys. Furthermore, the first-principles calculations

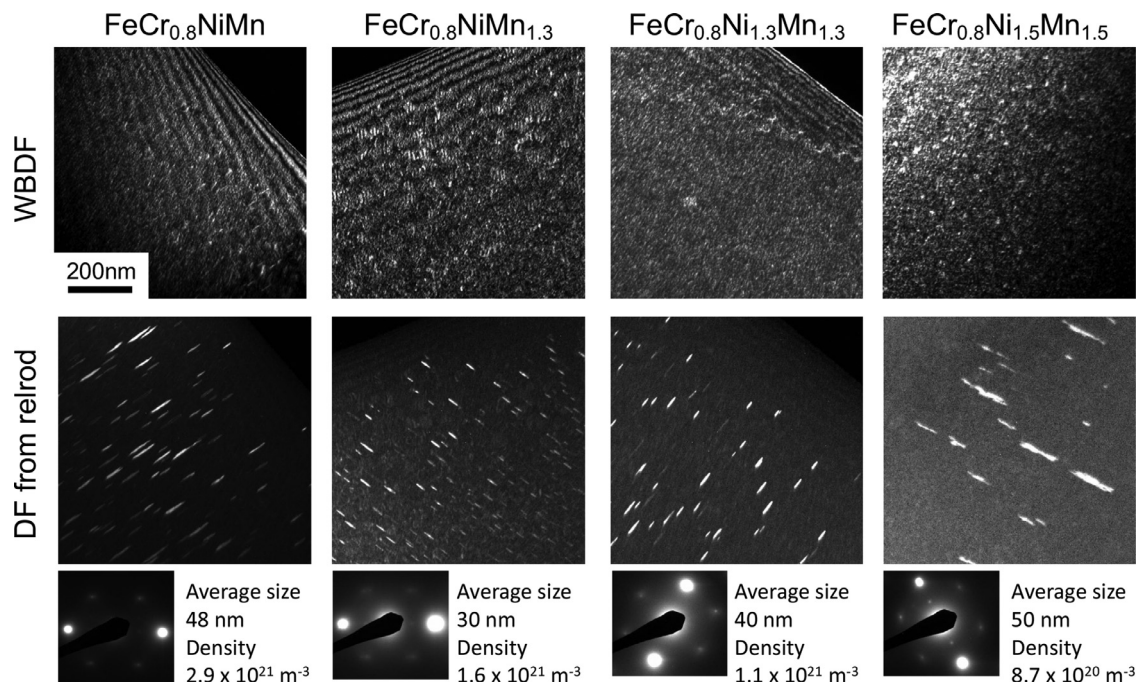


Fig. 6. Damage microstructure of irradiated  $\text{FeCr}_{0.8}\text{Ni}_x\text{Mn}_y$  alloys. BDs and FLs were observed in the WBDF images. The DF images from relrod showed only FLs on (111) plane.

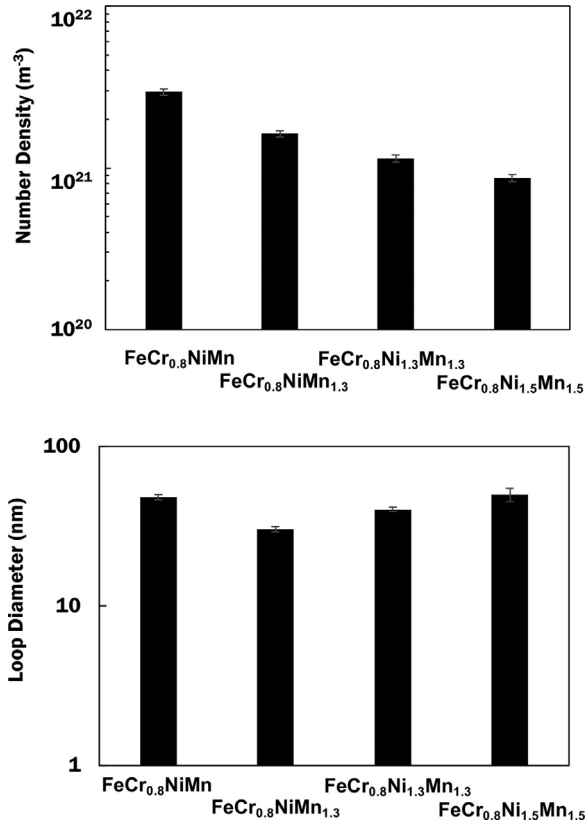


Fig. 7. Number density and average size of FL in irradiated  $\text{FeCr}_{0.8}\text{Ni}_x\text{Mn}_y$ . FL number density decreases with increasing Ni and Mn contents. While FL size is independent on element concentration.

indicated that the intrinsic SFE was predicted to monotonically increase with Mn content in paramagnetic FeMn alloys [29].

The increase in Mn and Ni contents resulted in the increase in SFE, but  $\sigma_{0.2}$ , UTS, and  $\varepsilon_t$  were almost the same in  $\text{FeCr}_{0.8}\text{Ni}_x\text{Mn}_y$  alloys. Generally, the lowering the SFE resulted in the increasing in the work-hardening rate and the deformation twinning formation [30]. In this study, however, less SFE dependence on Tensile property was shown in  $\text{FeCr}_{0.8}\text{Ni}_x\text{Mn}_y$  alloys.

The electron irradiation experiment resulted in the lowest FL number density in the irradiated  $\text{FeCr}_{0.8}\text{Ni}_{1.5}\text{Mn}_{1.5}$ , which had the

Table 3

Summary of FL number density ( $N$ ), FL average diameter ( $D$ ), and  $(ND)^{0.5}$  of irradiated  $\text{FeCr}_{0.8}\text{Ni}_x\text{Mn}_y$  alloys.

	Number density ( $N$ ) / $\text{m}^{-3}$	Average Diameter ( $D$ ) / nm	$(ND)^{0.5}$ / $\text{m}^{-1}$
$\text{FeCr}_{0.8}\text{NiMn}$	$2.9 \times 10^{21}$	48	$1.2 \times 10^7$
$\text{FeCr}_{0.8}\text{NiMn}_{1.3}$	$1.6 \times 10^{21}$	30	$6.9 \times 10^6$
$\text{FeCr}_{0.8}\text{Ni}_{1.3}\text{Mn}_{1.3}$	$1.1 \times 10^{21}$	40	$6.6 \times 10^6$
$\text{FeCr}_{0.8}\text{Ni}_{1.5}\text{Mn}_{1.5}$	$8.7 \times 10^{20}$	50	$6.6 \times 10^6$

highest SFE among  $\text{FeCr}_{0.8}\text{Ni}_x\text{Mn}_y$  alloys. G. Bellefon et al. reported that the SFE value in austenitic stainless steels was empirically evaluated as a function of the chemical composition [31]. The effect of Mn concentration on the SFE appeared to be more significant than the empirical dependence. The formation of SIA FL in FCC-type materials would be affected by the SFE in nature. A previous report indicated that the formation energy of SIA FL is dependent on SFE in nature; however, MD simulation could not indicate any SFE dependence on FL formation. While, on the SIA PL, the critical loop size is obviously dependent on SFE and becomes larger at lower SFE. Concerning about SFE in HEAs, Ni concentration dependence on SFE in  $\text{CoCrFeNiMn}$ -type HEAs in the range of 14–20 at% Ni [22] has been reported. In the case of the irradiated HEAs, the high Mn concentration in  $\text{CoCrFeNiMn}$ -type HEAs showed lower number density and smaller loop diameter of FL after  $\text{Kr}^+$  ion irradiation at 500 °C [19]. In this study, Co-free  $\text{FeCr}_{0.8}\text{Ni}_x\text{Mn}_y$  alloys also showed a similar tendency of the relationship between the FL formation and the SFE.

To correlate the irradiation hardening with microstructure, the Orowan hardening model [32] has been used. The formula is given as follows:

$$\Delta\sigma_y = M\alpha\mu b(ND)^{0.5}$$

where  $\Delta\sigma_y$  is the calculated increase in yield strength after irradiation.  $M$  is the Taylor factor (3.06 for equiaxed FCC),  $\alpha$  is the barrier strength factor (0.4 for FL) [33],  $\mu$  is the shear modulus (77 GPa for austenitic steels), and  $b$  is the Burgers vector of moving dislocation (0.257 nm).  $N$  and  $D$  are the number density and the size of obstacles, respectively, so that,  $\Delta\sigma_y$  can be estimated as a function of  $(ND)^{0.5}$ . The FL number density ( $N$ ) and the FL average diameter ( $D$ ), and  $(ND)^{0.5}$  of irradiated  $\text{FeCr}_{0.8}\text{Ni}_x\text{Mn}_y$  alloys are listed in Table 3. The value of  $(ND)^{0.5}$  seems to have the Mn and Ni concentration dependence. The values of  $(ND)^{0.5}$  in  $\text{FeCr}_{0.8}\text{Ni}_x\text{Mn}_y$  alloys were plotted as a function of the estimated SFE ( $\gamma$ ) in Fig. 9.

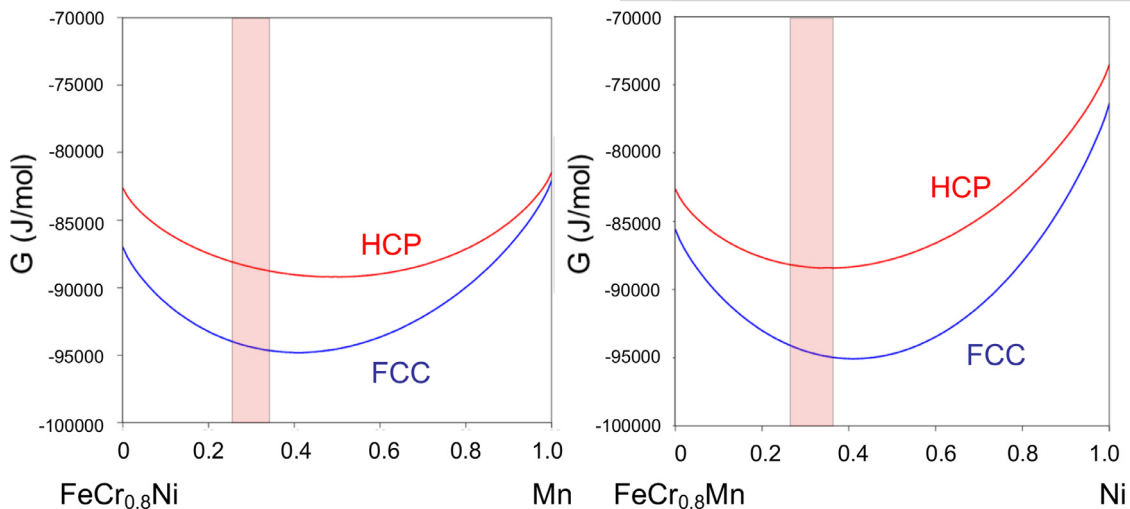


Fig. 8. Free energy change of FCC and HCP in  $\text{FeCr}_{0.8}\text{Ni}_x\text{Mn}$  and  $\text{FeCr}_{0.8}\text{NiMn}_x$  as a function of Ni and Mn contents, respectively.

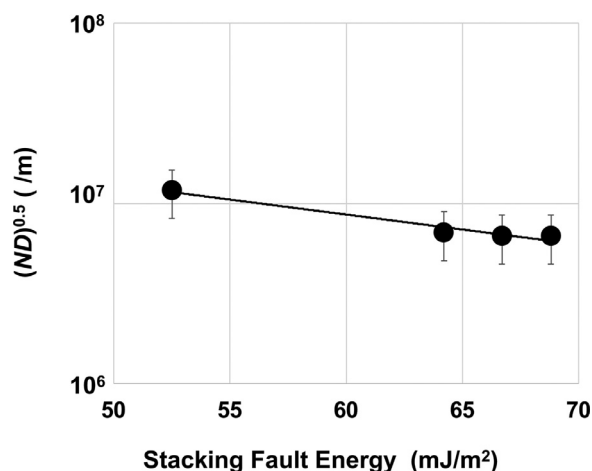


Fig. 9. The values of  $(ND)^{0.5}$  in  $\text{FeCr}_{0.8}\text{Ni}_x\text{Mn}_y$  alloys as a function of the estimated SFE ( $\gamma$ ).  $(ND)^{0.5}$  decreases with increasing SFE.

From this figure,  $(ND)^{0.5}$  can be formulated by following expressions.

$$(ND)^{0.5} = (9 \times 10^7) \exp(-0.038\gamma)$$

Considering that  $\text{FeCr}_{0.8}\text{Ni}_x\text{Mn}_y$  showed irradiation resistance compared to  $\text{CoCrFeNiMn}$  and 316SS, it can be expected that  $\text{FeCrNiMn}$ -based (Co-free) HEAs could be well-designed by controlling the SFE with optimized element concentration as one of candidate alloys for nuclear applications.

## 5. Summary

In order to clarify the effect of SFE on irradiation damage evolution in Co-free FCC-type HEAs, the effect of element content on the SFE and microstructure change in  $\text{FeCr}_{0.8}\text{Ni}_x\text{Mn}_y$  alloys were investigated by *in-situ* irradiation experiment.

The stacking fault energy of  $\text{FeCr}_{0.8}\text{Ni}_x\text{Mn}_y$  alloys was increased with increasing both Ni and Mn concentration,  $\text{FeCr}_{0.8}\text{Ni}_{1.5}\text{Mn}_{1.5}$  had the highest stacking fault energy, which was much higher value than that of 316SS. The electron irradiation at 400 °C resulted in the formation of faulted loops, but no observable voids in all the  $\text{FeCr}_{0.8}\text{Ni}_x\text{Mn}_y$  alloys. The comparison of microstructural evolution revealed less faulted loop formation in  $\text{FeCr}_{0.8}\text{Ni}_{1.3}\text{Mn}_{1.3}$  and  $\text{FeCr}_{0.8}\text{Ni}_{1.5}\text{Mn}_{1.5}$  alloys, leading to less irradiation hardening compared with a low SFE HEAs and 316SS. From these results, it is suggested that Fe CrNiMn-based HEAs would be one of candidate alloys as high irradiation resistant materials by controlling the stacking fault energy with optimized element concentration (Table 3).

## Declaration of Competing Interest

The authors declare that they have no known competing financial interests or personal relationships that could have appeared to influence the work reported in this paper.

## Acknowledgment

The authors appreciate the special support of Dr. Endo and the great helps of technical stuffs at Nano-Micro Materials Analysis Laboratory of Hokkaido University. This work was supported by JSPS Grant-in-Aid for Scientific Research on Innovative Areas Grant No. JP19H05161.

## References

- [1] J.W. Yeh, S.J. Lin, T.S. Chin, J.Y. Gan, S.K. Chen, T.T. Shun, C.H. Tsau, S.Y. Chou, Formation of simple crystal structures in Cu-Co-Ni-Cr-Al-Fe-Ti-V alloys with multiprincipal metallic elements, *Metall. Mater. Trans. A* 35 (2004) 2533–2536.
- [2] Y.J. Zhou, Y. Zhang, Y.L. Wang, G.L. Chen, Solid solution alloys of AlCoCrFeNiTiX with excellent room-temperature mechanical properties, *Appl. Phys. Lett.* 90 (2007) 181904.
- [3] C.Y. Hsu, J.W. Yeh, S.K. Chen, T.T. Shun, Wear resistance and high temperature compression strength of Fcc CuCoNiCrAl<sub>0.5</sub>Fe alloy with boron addition, *Metall. Mater. Trans. A* 35 (2004) 1465–1469.
- [4] C.M. Lin, H.L. Tsai, Equilibrium phase of high-entropy FeCoNiCrCu<sub>0.5</sub> alloy at elevated temperature, *J. Alloy. Compd.* 489 (2010) 30–35.
- [5] D.J.M. King, S.C. Middleburgh, A.G. McGregor, M.B. Cortie, Predicting the formation and stability of single phase high-entropy alloys, *Acta Mater.* 104 (2016) 172–179.
- [6] B. Komabaiah, K. Jin, H. Bei, P.D. Edmondson, Y. Zhang, Phase stability of single phase Al<sub>0.12</sub>CrNiFeCo high entropy alloy upon irradiation, *Mater. Des.* 160 (2018) 1208–1216.
- [7] T. Nagase, P.D. Rack, J.H. Noh, T. Nogami, *In-situ* TEM observation of structural changes in nano-crystalline CoCrCuFeNi multicomponent high-entropy alloy under fast electron irradiation by high voltage electron microscopy, *Intermetallics* 59 (2015) 32–42.
- [8] C. Lu, L. Niu, N. Chen, Ke Jin, T. Yang, P. Xiu, Y. Zhang, F. Gao, H. Bei, S. Shi, M.R. He, I.M. Robertson, W.J. Weber, L. Wang, Enhancing radiation tolerance by controlling defect mobility and migration pathways in multicomponent single-phase alloys, *Nat. Commun.* 7 (2016) 13564.
- [9] T. Yang, Congyi Li, Steven J. Zinkle, Shijun Zhao, Hongbin Bei, Yanwen Zhang, Irradiation responses and defect behavior of single-phase concentrated solid solution alloys, *J. Mater. Res.* 33 (19) (2018) 3077–3091, doi:10.1557/jmr.2018.285.
- [10] S.J. Zinkle, R.J.M. Konings (Ed.), Radiation-induced effects on microstructure, *Compr. Nucl. Mater.* 1 (2012) 65–98 vol..
- [11] G.S. Was, Materials degradation in fission reactors: Lessons learned of relevance to fusion reactor systems, *J. Nucl. Mater.* 367–370 (2007) 11–20.
- [12] M. Li, S.J. Zinkle, R.J.M. Konings (Ed.), Physical and mechanical properties of copper and copper alloys, *Compr. Nucl. Mater.* 4 (2012) 667–690 vol..
- [13] T. Muroga, H. Watanabe, Microstructure response in copper and copper alloys irradiated with fission neutrons with controlled temperature variations, *J. ASTM Int.* 1 (9) (2004) 1–10.
- [14] B.N. Singh, A. Horsewell, D.S. Gelles, F.A. Garner, Void swelling in copper and copper alloys irradiated with fission neutrons, *J. Nucl. Mater.* 191–194 (1992) 1172–1176.
- [15] F. Mota, I. Palermo, S. Laces, J. Molla, A. Ibarra, Potential irradiation of Cu alloys and tungsten samples in DONES, *Nucl. Fusion* 57 (12) (2017) 126056 vol..
- [16] R.M. Boothby, R.J.M. Konings, in: *Comprehensive Nuclear Materials*, 4, Elsevier, 2012, pp. 123–150.
- [17] W.Y. Chen, X. Liu, Y. Chen, J.W. Yeh, K.K. Tseng, K. Natesan, Irradiation effects in high entropy alloys and 316H stainless steel at 300 °C, *J. Nucl. Mater.* 510 (2018) 421–430.
- [18] N. Hashimoto, Y. Ono, Mobility of point defects in CoCrFeNi-base high entropy alloys, *Intermetallics* 133 (2021) 107182.
- [19] N. Hashimoto, T. Fukushi, E. Wada, W.Y. Chen, Effect of stacking fault energy on damage microstructure in ion-irradiated CoCrFeNiMn concentrated solid solution alloys, *J. Nucl. Mater.* 545 (2021) 152642.
- [20] C. Li, S.J. Zinkle, S. Zhao, H. Bei, Y. Zhang, Irradiation responses and defect behavior of single-phase concentrated solid solution alloys, *J. Nucl. Mater.* 527 (2019) 151838.
- [21] C. Parkin, M. Moorehead, M. Elbakhshwan, J. Hu, W.Y. Chen, M. Li, L. He, K. Sridharan, A. Couet, *In situ* microstructural evolution in face-centered and body-centered cubic complex concentrated solid-solution alloys under heavy ion irradiation, *Acta Mater.* 198 (2020) 85–99.
- [22] S.F. Liu, Y. Wu, H.T. Wang, J.Y. He, J.B. Liu, C.X. Chen, X.J. Liu, H. Wana, Z.P. Lu, Stacking fault energy of face-centered-cubic high entropy alloys, *Intermetallics* 93 (2018) 269–273.
- [23] G.H. Koo, J.H. Yoon, Inelastic material models of Type 316H for elevated temperature design of advanced high temperature reactors, *Energies* 13 (2020) 4548.
- [24] J. Gan, E.P. Simonen, S.M. Bruemmer, L. Fournier, B.H. Sencer, G.S. Was, The effect of oversized solute additions on the microstructure of 316SS irradiated with 5 MeV Ni ions or 3.2 MeV protons, *J. Nucl. Mater.* 325 (2004) 94–106.
- [25] D. Chen, K. Murakami, K. Dohi, K. Nishida, Z. Li, N. Sekimura, The effects of loop size on the unfauling of Frank loops in heavy ion irradiation, *J. Nucl. Mater.* 529 (2020) 15192 1–7.
- [26] T. Okita, Y. Yang, J. Hirabayashi, M. Itakura, K. Suzuki, Effects of stacking fault energy on defect formation process in face-centred cubic metals, *Philos. Mag.* 96 (2016) 1579–1597.
- [27] G.B. Olson, M. Cohen, A general mechanism of martensitic nucleation: Part I. General concepts and the FCC → HCP transformation, *Metall. Trans. A* 7 (1976) 1897–1904.
- [28] S. Lu, Q.M. Hu, B. Johansson, L. Vitos, et al., Stacking fault energies of Mn, Co and Nb alloyed austenitic stainless steels, *Acta Mater.* 59 (2011) 5728–5734.
- [29] Z. Dong, S. Schönecker, D. Chenb, W. Li, S. Lu, L. Vitos, Influence of Mn content on the intrinsic energy barriers of paramagnetic FeMn alloys from longitudinal spin fluctuation theory, *Int. J. Plast.* 119 (2019) 123–139.

- [30] S. Huang, W. Li, S. Lu, F. Tian, J. Shen, E. Holmström, L. Vitos, Temperature dependent stacking fault energy of FeCrCoNiMn high entropy alloy, *Scr. Mater.* 108 (44) (2015) 44–47.
- [31] G. Bellefon, J.C. van Duysen, K. Sridharan, Composition-dependence of stacking fault energy in austenitic stainless steels through linear regression with random intercepts, *J. Nucl. Mater.* 492 (2017) 227–230.
- [32] E. Orowan, G.M. Rassweiler, W.L. Grube, in: *Internal Stresses and Fatigue in Metals*, Elsevier Science Publication, 1959, pp. 59–80.
- [33] T.S. Byun, N. Hashimoto, K. Farrell, E. Lee, Characteristics of microscopic strain localization in irradiated 316 stainless steels and pure vanadium, *J. Nucl. Mater.* 349 (3) (2006) 251–264.